System Identification and Control of Mechanical Samara Micro-Air-Vehicles

Evan R. Ulrich, J. Sean Humbert, and Darryll J. Pines*

Micro/Nano Unmanned Aerial Systems (UAS) are an emerging class of vehicles uniquely suited to performing covert missions. Autonomy is an essential aspect of the intended function of UAS, and development of a dynamic model will enable control and state estimation algorithm synthesis. To that end, a linear model for the heave dynamics of a mechanical samara (winged seed) in hovering flight was identified from data collected external to the vehicle by a visual tracking system. Identification and error estimation efforts utilized a frequency response-based system identification. The two mechanical samara vehicles of differing scale compared in this study represent the first demonstration of controlled flight of a vehicle of this kind.

I. Nomenclature

θ_0	Control Input	$norm$
x, y, z	Inertial Frame Position	m
ϕ, θ, ψ	Euler Angles	rad
u, v, w	Translational Velocities	m/s
p, q, r	Rotational Velocities	rad/s
R_{BF}	Direction Cosine Matrix	rad
K_d	Derivative Gain	
K_p	Proportional Gain	
K_i	Integral Gain	
ϵ_i	Infinitesimal Quantity	
I_x, I_y, I_z	Principal Moments of Inertia	$Kgmm^2$
Z_w	Heave Stability Derivative	$1/s$
Z_{θ_0}	Collective Input Stability Derivative	m/s^2
$\dot{w}$	Heave Acceleration	m/s^2
λ	Roots of Characteristic Equation	

II. Introduction

IN recent years a new paradigm of flight has emerged which encompasses micro-scale aircraft that are bio-inpired. These highly maneuverable platforms are capable of hovering flight and are ideally suited for operation in a confined environment. The reconnaissance mission envisioned requires a high level of autonomy due to the fast dynamics of the vehicle and the limit on communication in the likely areas of operation, i.e. caves and buildings. Development of a state space model of the system dynamics about a trimmed flight condition will facilitate future model-based controller and observer design enabling autonomous operation.

Aerial systems which satisfy the dimensional constraints outlined by the DARPA "Micro Air Vehicle" (MAV) initiative include fixed-wing, rotary-wing and flapping-wing vehicles. The simplest and most mature

*Evan R. Ulrich and J. Sean Humbert are with the Department of Aerospace Engineering, Darryll J. Pines is the Dean of Engineering, University of Maryland, College Park, MD 20742 USA

of these platforms are fixed-wing vehicles which boast speed, simplicity and well-known dynamics, however the limitation of forward flight restricts functionality in cluttered environments that can be traversed by rotary and flapping-wing platforms. Micro-scale helicopter linear dynamic system models have been described by Conroy et al,[1] using system identification tools developed by Tischler[2] and Mettler[3] for substantially larger vehicles including the Yamaha RMAX helicopter.

A substantial challenge in modeling the dynamics of micro-scale flight is the general lack of knowledge of the complex low Reynolds number flow regime they inhabit. Additionally the vehicles are highly susceptible to wind gusts as a result of low vehicle inertia. The complexity of the system can be reduced substantially by identifying a linear model which describes its reaction to forces imposed by a control input. A model description of this nature lends itself well to modern control and state estimation.

The intent of this manuscript is to characterize the flight dynamics and control of a rotary-wing MAV based on one of natures most efficient fliers: the seed of the maple (Acer) tree or samara. Identification and error estimation of the vehicle dynamic model was done with data collected by a visual tracking system,[4] and utilization of a frequency response-based system identification package developed at the Army Aeroflightdynamics Directorate (AFDD) located at Moffett Field, CA. Frequency domain system identification is limited to linear models valid only for small perturbations about the trimmed condition.

Model structure is based on a reduction of the longitudinal dynamics of a helicopter in hover to a linear system described by stability derivatives. Cramer Rao insensitivity bounds describe the likely error resulting from multiple trials and is used to validate the estimates of the identified parameters. Additional validation of the linear model is done through implementation of a linear controller with feedback provided by the visual tracking system.

III. Vehicle Description

The concept of a single-wing rotating aircraft is not a new one, and in fact the first vehicle of this type was flown in 1952 in the woods surrounding Lake Placid, New York by Charles W. McCutchen .[5] A more recent vehicle was developed and flown by a team led by Lockheed Martin Advanced Technology Laboratories .[6] The prototype called MAVPro incorporated an outrunner motor with an 8 inch diameter propeller, weighed 514 grams, rotated at a stable 4 Hz, and could climb to 50 ft with radio controlled actuation of a trailing edge flap. The MAVPro incorporated the AG38 airfoil, and exhibited a rectangular planform geometry. The various single winged rotating aircraft developed over the years have made no attempt to utilize the most basic mode of transit of natural samara, autorotation. Additionally, airfoil cross sections and planform designs have had no similarity to that found in natural samaras.

The authors intent in the design of the vehicles discussed herein was to emulate the natural samara, and in doing so take advantage of the highly efficient autorotation which it employs. As such, samara-I and samara-II use unconventional and samara-inspired planform geometry and airfoil cross-sections developed previously by the authors.[4] The sign convention and corresponding vehicle orientation is shown in Figure 5. These vehicles perform stable autorotation and are capable of landing at terminal velocity without sustaining any damage. In the event of motor failure, the vehicles gently autorotate back to the ground. Conventional monocopter designs apply torque to the vehicle with a thrust device slightly off-set from the Y-axis, and in the case of MAVPro the propeller spins in the Y-Z plane and influences the stability about the Y-axis. This configuration results in the propeller fighting the pitch input from the flap and reduces controllability of the vehicle. The 5-inch diameter propeller of the samara-I,II is spinning in the X-Z plane and opposes applied torque about the X-axis providing additional stability.

The design and construction of the samara used in these experiments was done with the intent of providing a stable vehicle that could be tested in a limited area. The unconventional wing and body structure are the result of an iterative design process which has produced on the order of one-hundred vehicles. The resultant vehicles are extremely damage tolerant as they employ flexible structures which deflect upon impact, effectively increasing the time over which the impact load is applied to the vehicle. The configuration and relative size of the vehicles are shown in Figure reff:flightconfig. Advantages over traditional micro-scaled VTOL configurations include passive stability, efficient autorotation, low body drag, mechanical simplicity, low cost, high payload capacity, and substantial damage tolerance.

The design and construction of the samara used in these experiments was done with the intent of providing a stable vehicle that could be tested in a limited area. The unconventional wing and body structure are the result of an iterative design process which has produced on the order of one-hundred vehicles. The

resultant vehicles are extremely damage tolerant as they employ flexible structures which deflect upon impact, effectively increasing the time over which the impact load is applied to the vehicle. The configuration and dimensions of the vehicles are shown in Figure 1. Advantages over traditional micro-scaled VTOL configurations include passive stability, efficient autorotation, low body drag, mechanical simplicity, low cost, high payload capacity, and substantial damage tolerance.

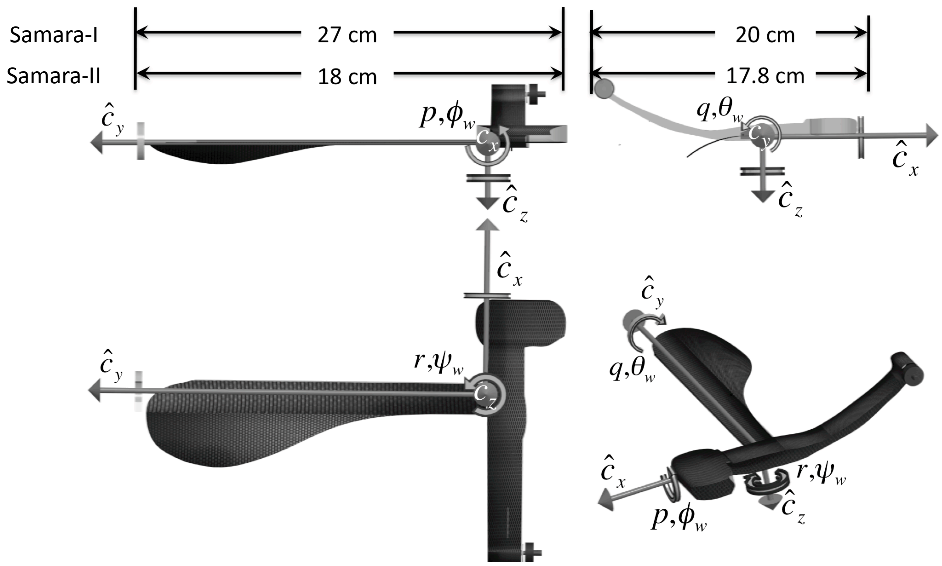

Figure 1. Roll, Pitch and Yaw definitions for body fixed coordinate system

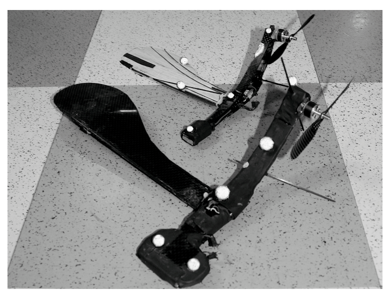

Figure 2. Samara in Flight Configuration

IV. Vehicle Design

The primary load-bearing structure of the vehicle is 0/90 ply .025 thick carbon-fiber composite laminate, with opposed parallel tension and compression members mounted to the motor and wing. In this configuration the structure provides a high degree of flexure in the Z-direction and a high degree of stiffness in the plane of rotation. The angle at which the motor is held provides protection from ground impingement on take-off and landing.

Flight time of the samara-I is roughly 20 minutes with a 0.025 Kg, 480mAh 7.4 V two-cell Lithium-Polymer battery, for a total vehicle mass (GW) of 0.075 Kg. The maximum gross take-off weight (GTOW) of the vehicle is 0.125 Kg, and the maximum dimension is 0.27 m, Figure 1. The second and smaller samara tested, called samara-II is designed and constructed in a similar fashion to samara-I, however the total mass is 0.038 kg, and maximum dimension is 0.18 m, Figure 1. Table 1 details the mass breakdown of samara-I,II as well as two hobby radio controlled rotorcraft. The mass breakdown is similar for the four vehicles, however the samara benefits from a less complex and therefore lighter Propeller/Rotor system and require no transmission as it directly drives the propeller. This decrease in complexity creates a more robust and

Table 1. Weight Data (In terms of percent of GW)

Parameter	samara-II	samara-I	Hobby Rotorcraft 1	Hobby Rotorcraft 2
Mass	0.038 Kg	0.075 Kg	0.3 Kg	1.8 Kg
Maximum GTOW	.048 Kg	.125 Kg		
Maximum Dimension	.18 m	.27 m		
Percent Gross Weight	GW	GW	GW	GW
Propeller/ Rotor System	5.3	2.6	11.0	11.2
Tailboom Assembly	2.6	3.3	8.0	9.1
Main Motor (electric)	10.5	10.7	15.4	10.5
Fuselage/ structure	26.3	27.6	7.0	15.1
Main Transmission	Direct drive	2.0	3.4	
Landing Gear	2.6	2.7	2.3	3.4
Control System	18.4	16	5.7	18.3
Flight Control Avionics	7.9	4	29.4	2.4
Power Source	26.3	33.3	19.2	26.6
Payload	0	0	0	0
Flight Time	10min	20min		

reliable system.

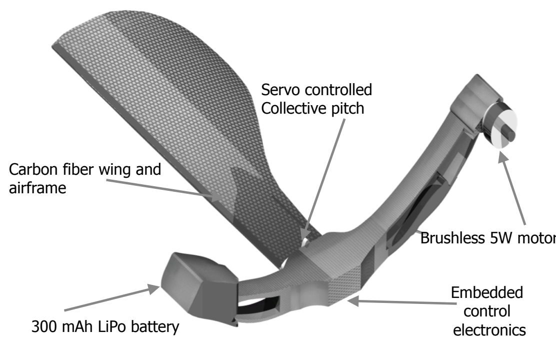

Figure 3. Robotic samara component diagram

V. Stability Properties

A substantial advantage of the samara-I vehicle is that it is a passively stable system. A simple qualitative stability analysis of the samara-I in a steady hover, or autorotation illustrates this point. In a steady hover the thrust from the propeller is balanced by the drag from the body and wing, resulting in a near constant rotational rate about its principal inertial axis, I_z. Alternatively, in autorotation the resistive torque of the wing drag is equal to the driving torque of the lift, for a net zero torque. Consider the assumed motion $r = r_0$ and $p, q << r_0$ in steady hover, or autorotation. To investigate whether the motion is stable or not, neglecting aerodynamic contributions, a small moment is applied to the body such that after the moment is applied the resultant angular velocities are as follows:

$$p = \epsilon_p \tag{1}$$

$$q = \epsilon_q \tag{2}$$

$$r = r_0 + \epsilon_r \tag{3}$$

Where $\epsilon_i (i = 1, 2, 3)$ are infinitesimal quantities. To determine the evolution of these perturbed angular velocities in time it is convenient to use the Euler equations as follows:

$$I_z(\dot{r}_0 + \dot{\epsilon}_r) + (I_x - I_y)\epsilon_p \epsilon_q = 0 \tag{4}$$

$$I_x \dot{\epsilon}_p - (I_y - I_z)(r_0 + \epsilon_r)\epsilon_q = 0 \tag{5}$$

$$I_y \dot{\epsilon}_q - (I_z - I_x)(r_0 + \epsilon_r)\epsilon_p = 0 \tag{6}$$

The change in angular velocities is small, and as such allows linearization of the above equations by eliminating quadratic and higher order terms in ϵ_i yielding:

$$I_z \dot{\epsilon}_r = 0 \tag{7}$$

$$I_x \dot{\epsilon}_p - (I_y - I_z) r_0 \epsilon_q \tag{8}$$

$$I_y \dot{\epsilon}_q - (I_z - I_x) r_0 \epsilon_p \tag{9}$$

This implies ϵ_r is constant. The behavior of the remaining angular velocities can be understood with eigenvalue analysis. Assuming a solution of the form:

$$\epsilon_p(t) = E_p e^{\lambda t} \tag{10}$$

$$\epsilon_q(t) = E_q e^{\lambda t} \tag{11}$$

Next, we can introduce the expansions into the linearized equations:

$$\begin{bmatrix} I_x \lambda & (I_z - I_y) r_0 \\ (I_x - I_z) r_0 & I_y \lambda \end{bmatrix} \begin{bmatrix} E_p \\ E_q \end{bmatrix} e^{\lambda t} = \begin{bmatrix} 0 \\ 0 \end{bmatrix} \tag{12}$$

The solution requires that the determinant of the coefficient matrix be zero, which yields the characteristic equation:

$$I_x I_y \lambda^2 - (I_x - I_z)(I_z - I_y) r_0^2 = 0 \tag{13}$$

The solution is:

$$\lambda = \pm i \sqrt{\frac{(I_x - I_z)(I_z - I_y) r_0^2}{I_x I_y}} \tag{14}$$

Two types of solutions are possible and depend on the principal moments of inertia. If $I_x > I_z$ and $I_y > I_z$, or if $I_x < I_z$ and $I_y < I_z$ (characteristic of samara-I and samara-II) both roots of the characteristic equation are imaginary. In the absence of nonconservative forces, the system is marginally stable.[7] The inertial parameters of the samara vehicles as well as the resultant eigenvalues are listed in Table 2.

Table 2. Inertia properties, rotation rate, and resultant eigenvalues for samara-I and samara-II

	I_x	I_y	I_z	r_0	λ	
	$Kgmm^2$	$Kgmm^2$	$Kgmm^2$	rad/sec		
samara-I	248	562	797	80.5	$0 + 77i$	rad/sec
samara-II	35	98	122	76	$0 + 59i$	rad/sec

VI. Experimental Setup

A. Visual Tracking System

Position and orientation of each vehicle was collected at a rate of 500 Hz, using a Vicon visual tracking system. During a flight test, the tracking system utilizes eight cameras to track the three-dimensional position of three retro-reflective markers placed on the samara wing. Each marker is spherical with a diameter of 5 mm. The three dimensional shape of the marker allows for better tracking by the Vicon system. A model of the vehicle geometry and the exact locations of the markers are used for least-squares estimates of the position of the center of mass. Figure 4 displays images of the virtual capture volume and the rigid body dynamic model of the samara wing created by the retro-reflective markers.

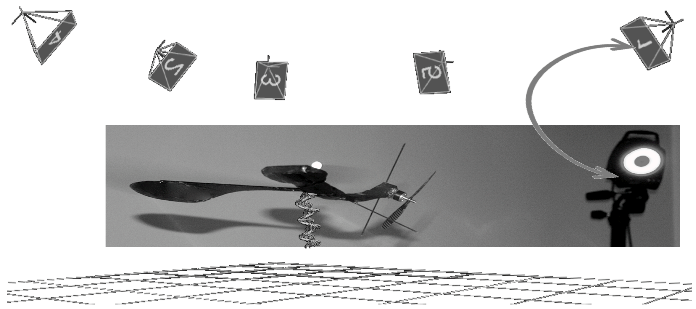

Figure 4. Representative VICON workspace and flight path of samara-II

B. Telemetry Synchronization

Pitch input is measured by two methods, both on, and off-board the vehicle. The state of the actuator is measured off-board the samara on an identical system receiving commands from the same transmitter. Two markers are placed on an arm attached to the off-board actuator to track the input to the vehicle. During a flight test the samara vehicle and the off-board actuator are simultaneously tracked allowing the angular displacement measured on the ground to be correlated to the motion of the samara vehicle, both of which are synchronized in time. Available Inputs and Outputs for Identification

C. Vehicle Inputs

It is advantageous to track the wing pitch angle via the off-board system as it provides the ability to track the collective inputs when the vehicle is not flown within the capture volume of the Vicon vision system. The on-board method includes measuring both pitch angle, θ, and coning angle, β, via the markers placed on the wing. It is interesting to compare the on-board and off-board measurements as the on-board angles are influenced by the aerodynamic forces acting on the vehicle. Nothing was presumed to be known about what forces or deflection angles were generated given a change in the actuator, therefore all control inputs are normalized. The input command is given by θ_0 for collective input and is normalized such that $\theta_0 \in [-1, 1]$.

D. Kinematic Output

The Vicon obtained estimates are exceptionally low noise as compared to commercial grade on-board attitude estimation sensors. The position noise variance was estimated by recording data while not moving the vehicle, and is shown in Table 3. The low noise presence in the position estimate allows the inertial position to be

Table 3. Measurement Characteristics

Measurement	Symbol	Source	Resolution	Variance	Unit
Time	t	VPS	$1.000 \times 10 - 3$	-	s
Control Input	θ_0	VPS	-	$7.8000 \times 10 - 3$	$norm$
Position	x, y, z	VPS	-	$0.613 \times 10 - 3$	m
Orientation	ϕ,θ,ψ	VPS	-	$7.800 \times 10 - 3$	rad
Translational Velocity	u, v, w	VPS	-	$0.251 \times 10 - 3$	m/s
Rotational Velocity	p, q, r	VPS	-	$1.200 \times 10 - 3$	rad/s

numerically differentiated to yield inertial velocity estimates.

$$\{\dot{X}, \dot{Y}, \dot{Z}\}^T = \frac{\partial}{\partial t}\{X, Y, Z\}^T \tag{15}$$

The body fixed velocities can be directly computed using the direction cosine matrix representation of the orientation estimate, RBF, and the inertial velocities as:

$$\{u, v, w\}^T = R_{BF}\{\dot{X}, \dot{Y}, \dot{Z}\}^T \tag{16}$$

E. Attitude Representation:

The transformation from the inertial frame to that of the body frame is described by three Euler angles, and is standard for aircraft. The transformation matrix can then be written as:

$$R_{BF} = \begin{bmatrix} c\psi c\theta & s\psi c\theta & -s\theta \\ c\psi s\theta s\phi - s\psi c\phi & c\psi c\phi + s\psi s\theta s\phi & c\theta s\phi \\ s\psi s\phi + c\psi s\theta c\phi & s\psi s\theta c\phi - c\psi s\phi & c\theta c\phi \end{bmatrix} \tag{17}$$

The notation is such that $s\theta = \sin\theta, c\theta = \cos\theta$. This rotation sequence is standard for aircraft.[8] The Euler angular rates are defined in the inertial coordinate system, Figure 5. The angular rates in the inertial frame are finite rotations, which do not commute, it is thus necessary to define the body angular rates separately. The sum of the inner products of each of the inertial angular rates with the body axis of interest yields the body angular rates:

$$p = -\dot{\psi}\sin\theta + \dot{\phi} \tag{18}$$

$$q = -\dot{\psi}\cos\theta\sin\phi + \dot{\theta}\cos\phi \tag{19}$$

$$r = -\dot{\psi}\cos\theta\cos\phi - \dot{\theta}\sin\phi. \tag{20}$$

A schematic detailing the axis of these rotations is shown in Figure 5. The 3D marker position data provides

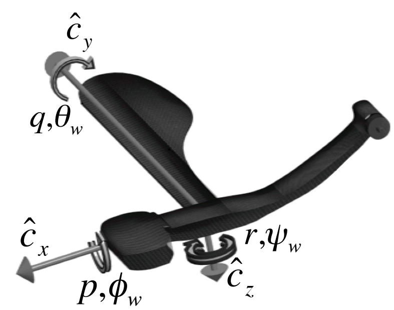

Figure 5. samara coordinate system

a means of resolving the orientation of the mechanical samara in space. The three markers are sufficient to describe an orthonormal basis from which the rotation matrix representing the samaras orientation can be formed.

F. Open-Loop Flight Test Data

The first step in a system identification is to pilot the vehicle in a flight envelope where the dynamics of interest are thoroughly excited. The vehicle was piloted within the capture volume of the vision system while simultaneously collecting the inputs and vehicle kinematics. The pilot attempted to excite the vehicle over a wide range of frequency content to best determine the relationship between input and output. For proper system identification, it is important to collect flight data open loop as a closed loop feedback system would alter the natural dynamics of the vehicle. The open loop setup is shown in Figure 6. Typical portions from

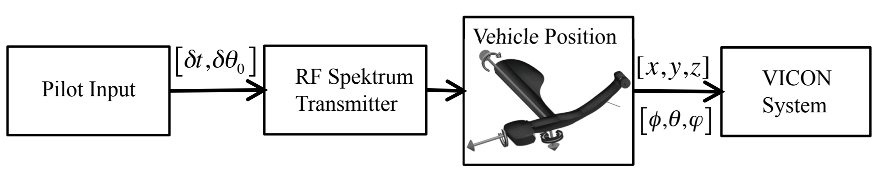

Figure 6. Open-loop control setup

recorded open loop data sets are shown in Figure 7. The heave velocity, w, is found by applying the central difference approximation to the vehicle vertical position data collected by the Vicon system. Figure 7 also compares the inputs given to the vehicle during one flight test as calculated both on-board and off-board the mechanical samara. Both on-board and off-board methods demonstrate similar pitch inputs, but the on-board measurements display more oscillations, demonstrating the effects of the aeroelastic forces acting on the wing.

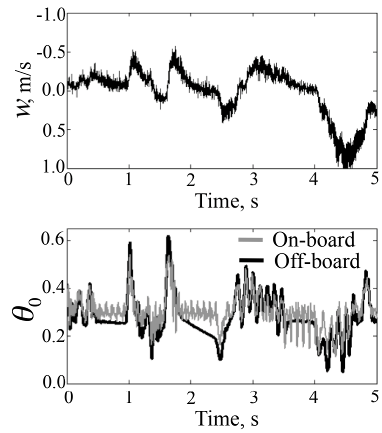

Figure 7. Flight data collected on samara-I

G. Closed-Loop Flight Test Data

Implementation of closed loop flight is enabled by an off-board feedback system. The ground control station setup is shown in Figure 8. During closed loop flight, the position and orientation of the mechanical samara are tracked by the Vicon visual system, which sends the information to a LabVIEW controller program.[9] The LabVIEW program takes into account the vehicles vertical position and heave velocity to create wing collective commands which are sent through a PIC 18F8722 microcontroller. The PIC microcontroller in turn sends the commands to the vehicle through a Spektrum Transmitter.

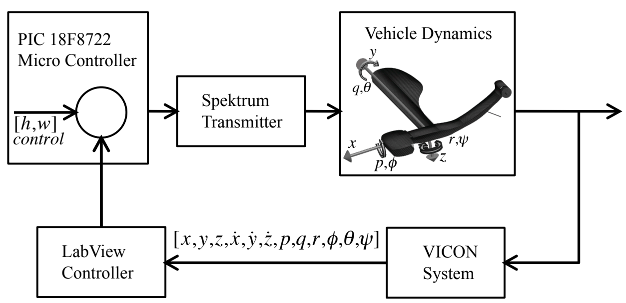

Figure 8. Ground Control Station (Closed Loop)

VII. Experimental Results

A. System Identification Method

A beneficial step in the identification process is computing the coherence function. This step provides a measure of the extent to which an output is linearly related to the input over some frequency range .[2] The magnitude squared coherence is given by:

$$\gamma_{xy}^2(\omega) \equiv \frac{|R_{xy}(\omega)|^2}{|R_{xx}(\omega)||R_{yy}(\omega)|} \tag{21}$$

where R_{xy} is the cross spectral density between the input and output, R_{xx} is the auto-spectral density of the input and R_{yy} is the auto-spectral density of the output. An input/output pair with low coherence implies either the input has no effect on the output or the effect is nonlinear. However, an input/output pair with high coherence implies the relationship can be modeled well by a linear model such as a transfer function or state space model. Tischler [2] suggests a coherence of 0.6 or above for some useful frequency range is necessary for accurate transfer function identification. The magnitude squared coherence for the

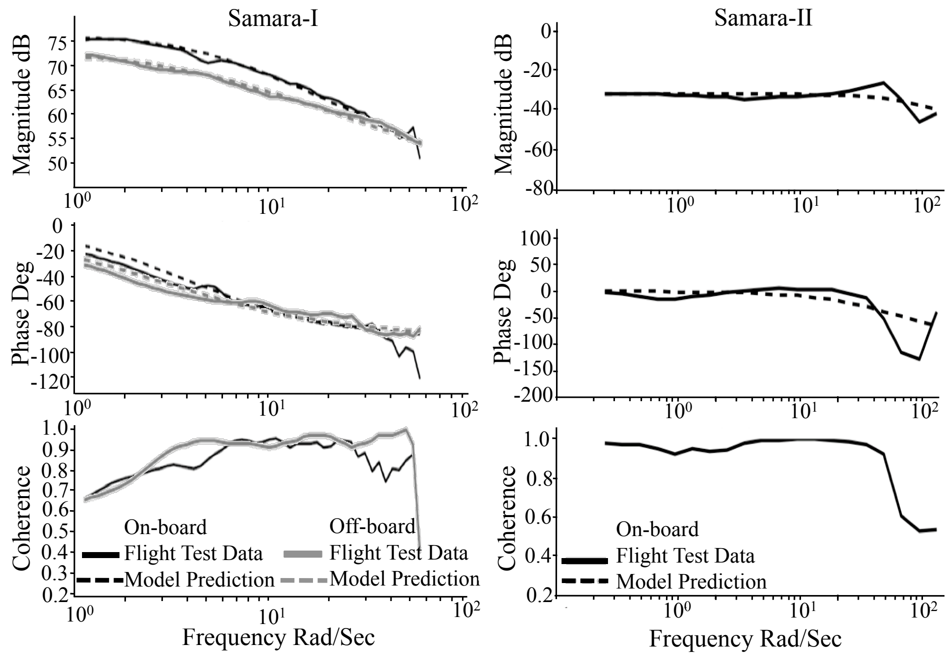

Figure 9. samara-I,II Identified model Bode diagram with corresponding data coherence, for On-board and Off-board data collection and transfer function $G(s) = \frac{K}{s - T_{pl}}$

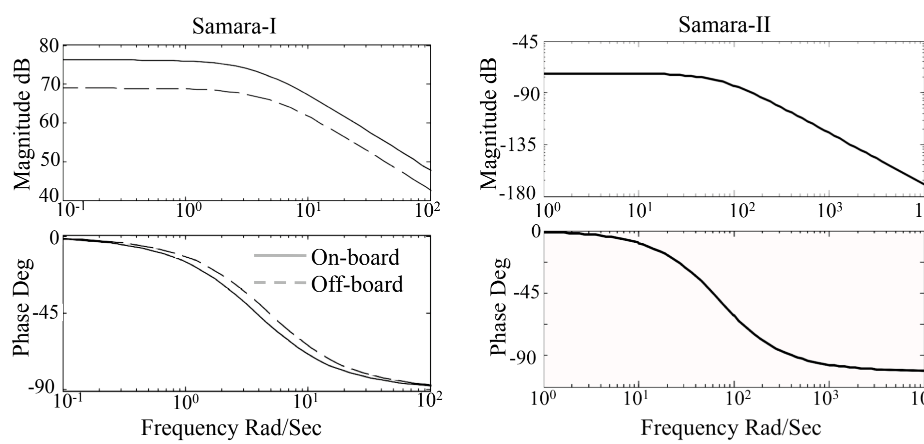

Figure 10. samara-I,II Identified model Bode diagram, for On-board and Off-board data collection and transfer function $\dot{w} = Z_w w - Z_{\theta_0 \theta_0}$

input/output relationship of samara-I using the on-board actuator system for input measurement is shown in Figure 9. It can be seen that the useful frequency for this input/output pair lies in the range of about 0.3 to 10 Hz. The coherence and useful frequency range predicted by the on-board measured θ_0 is equivalent to that of the off-board measurement, Figure 9. The similarity of the two predictions validates the hypothesis that off-board measurements of θ_0 are capable of capturing the physics relevant for system identification. The on-board measurement of θ_0 for samara-II demonstrates some high frequency behavior above 55 rad/sec and may be a result of the aeroelasticity of the wing in flight, Figure 9. All three coherence plots demonstrate similar ranges for strong relationships between input and output.

B. Open Loop Control

The transfer function, G, of the pitch input to heave dynamics was modeled as a first-order continuous-time process model:

$$G(s) = \frac{K}{s - T_{pl}} = \frac{W(s)}{\Theta(s)} \tag{22}$$

where K is the static gain and T_{pl} is a time constant. Given a flight data set with sufficient coherence, as seen in Figure 9, the MATLAB System Identification Toolbox[10] can be used to complete frequency response-based system identification. The input and output data is imported to the system identification GUI where it is filtered to 100 rad/sec using a fifth-order Butterworth filter. Table 4 shows the values identified for the Mechanical samara for the collective to heave velocity transfer function using data from both methods of measuring pitch input. In comparing the two methods of identification, it is important to note that both methods identify K and T_{pl} to be on the same order of magnitude, proving both methods have similar capabilities in capturing the input-output relationship. The transfer functions of the computed models are plotted in Figure 10,9.

Table 4. Identified robotic samara parameters

	samara-I	samara-I	samara-II
θ_0	Off-board	On-board	On-board
K	-13.643	-24.689	-21.44
T_{pl}	-4.864	-3.814	-1.690

C. Error analysis

A state space model was created allowing for error estimation using the Cramer-Rao bounds, and is represented as

$$\dot{x} = Ax + Bu \tag{23}$$

$$y = Cx \tag{24}$$

Where x is the state vector, A is the dynamics matrix, B is the control matrix, and C is the output matrix. The state space model for this identification reduces to

$$\dot{w} = Z_w w - Z_{\theta_0 \theta_0} \tag{25}$$

where is the heave acceleration, Zw is the stability derivative for heave velocity and is the collective input control derivative. The Cramer-Rao bounds are theoretical minimum limits for the expected standard deviation in the parameter estimates which would be obtained from several experiments.[2] Tischler suggests the following conditions represent the most valid parameter estimates:

$$CR\%20\% \tag{26}$$

$$\bar{I}\%10\% \tag{27}$$

The CR and $\bar{I}$ percentages were found using the Comprehensive Identification of FRequency Responses software (CIFER).[11] Table 5 shows the parameter estimates and associated error bounds of the identified state space model. The table demonstrates the validity of the identified parameter estimates, as all parameters meet the conditions specified. Table 5 : The model computed from both on/off-board measurement of the collective angle input is capable of capturing most of the low frequency inputs, but can be seen to average higher frequency excitation. The model computed from the off-board measurement of collective angle input performs well at the lower frequencies, but tends to average the higher frequency excitation. The model tends to exhibits more overshoot than that of the model derived from on-board measurements. The small differences in the performance of the two methods of input measurement validate the ground based input observation method. A comparison of the poles identified by MATLAB and CIFER is displayed in Figure 11. The control derivative is a negative number as an increase in collective pitch results in an increase in rotor thrust.

Table 5. **Mechanical samara Identified Parameter with Cramer-Rao Error Estimates.**

	Term	Value	$CR\%$	$\bar{I}\%$
On-board samara-I	Z_w	-6.382	10.04	4.231
-	Z_{θ_0}	-15.880	4.733	1.994
Off-board samara-I	Z_w	-4.303	9.413	3.808
-	Z_{θ_0}	-28.130	5.022	2.032
On-board samara-II	Z_w	-20.640	13.670	2.064
-	Z_{θ_0}	-1.501	12.840	1.939

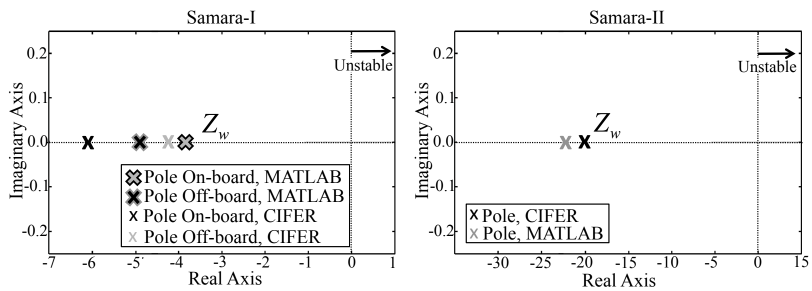

Figure 11. Real negative heave pole for samara-I,II

D. Heave Dynamics

The heave dynamics of the mechanical samara in hover are described by

$$\dot{w} - Z_w w = 0, \tag{28}$$

which has the analytical solution

$$w(t) = w_0 e^{Z_w t}. \tag{29}$$

Because the stability derivative Z_w is negative, the motion following a heave perturbation is a stable subsidence, shown in Figure 12. For example, a positive heave perturbation will generate an upflow through the mechanical samara rotor disk and increase thrust which acts in the negative direction of the z-body axis. This also implies that in hover the mechanical samara will have a real negative pole, as shown in Figure 11. It is now possible to obtain the expression for altitude loss due to a velocity perturbation w_0. For a

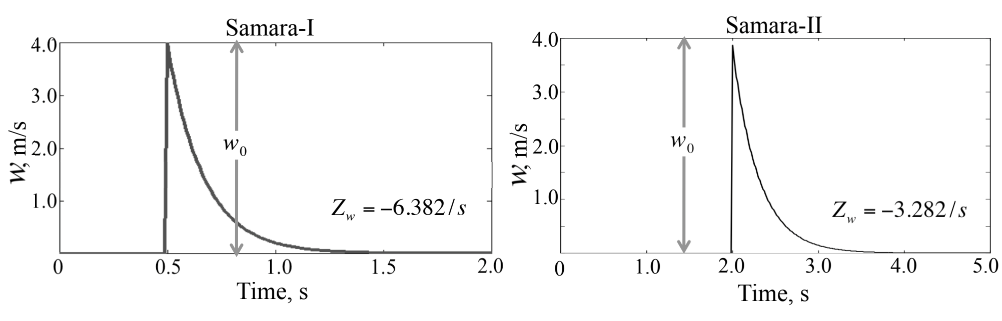

Figure 12. Motion following a perturbation w_0 of heave velocity

mechanical samara in hover $w = \dot{Z}$ and

$$z(t) = \int_0^t w dt + z_0 = w_0 \int_0^t e^{Z_w t} dt + z_0 \tag{30}$$

where z_0 is the initial altitude. Integrating from $\{0, t\}$ yields

$$z(t) = z_0 - \frac{w_0}{Z_w}[1 - e^{Z_w t}]. \tag{31}$$

For which the asymptotic value of altitude loss is

$$\lim_{t\infty} = -\frac{w_0}{Z_w} \tag{32}$$

The mechanical samara altitude change in response to a perturbation of heave velocity is shown in Figure 13.

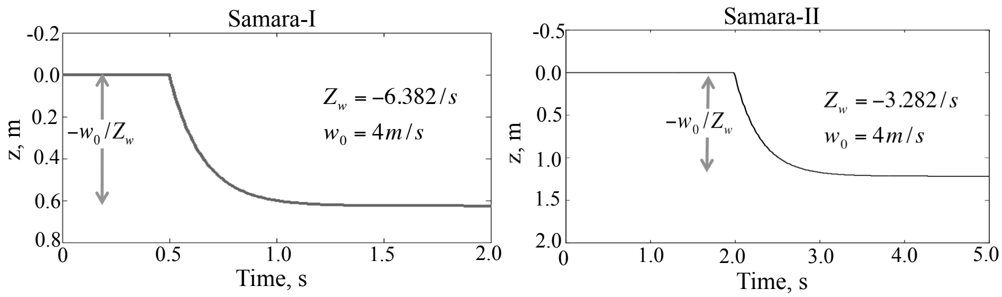

Figure 13. Motion following a perturbation w_0 of heave velocity

E. Heave response to pilot input

Consider a step input of collective pitch θ_0, after which $\theta_0 = conts$. After a change of variables the heave dynamic equation can be written as

$$\dot{w}_1 - Z_w w_1 = 0 \tag{33}$$

where

$$w_1(t) = w(t) + \frac{Z_{\theta_0}}{Z_w}\theta_0, \dot{w}_1 = \dot{w}. \tag{34}$$

The analytic solution of the first order differential equation is

$$w_1(t) = w_{1_0} e^{Z_w t}, \tag{35}$$

with $w_{1_0} = \{w + \frac{Z_{\theta_0}}{Z_w}\theta_0\}_{t=0^+}$. For the mechanical samara in a steady hover $w = 0$, which reduces the solution of $w_1(t)$ to

$$w_1(t) = \frac{Z_{\theta_0}}{Z_w}\theta_0 e^{Z_w t}. \tag{36}$$

Thus the heave velocity response to a step input of collective pitch reduces to

$$w(t) = -\frac{Z_{\theta_0}}{Z_w}\theta_0(1 - e^{Z_w t}). \tag{37}$$

An example of the first order character of the vertical speed response to a step input of collective pitch is shown in Figure 14. This is a basic characteristic of the behavior of a mechanical samara, and is clearly identifiable in results obtained from mathematical models and flight tests.

F. Closed Loop Feedback Control

Feedback control is used to correct for perturbations in the system in order to keep the vehicle at a reference condition. The structure of the closed loop system is depicted in Figure 15 $G_p(s)$ is the plant transfer function, $K(s)$ is the controller, Y_d is the reference value, and Y is the output. Precise attitude data is collected by the VICON motion capture system. The commanded altitude of the samara is maintained by feeding back the error in position to a control loop which contains the system and actuator dynamics. The closed loop system attempts to compensate for errors between the actual and reference height of the samara by measuring the output response, feeding the measurement back, and comparing it to the reference value at the summing junction. If there is a difference between the output and the reference, then the system drives the plant to correct for the error.[12]

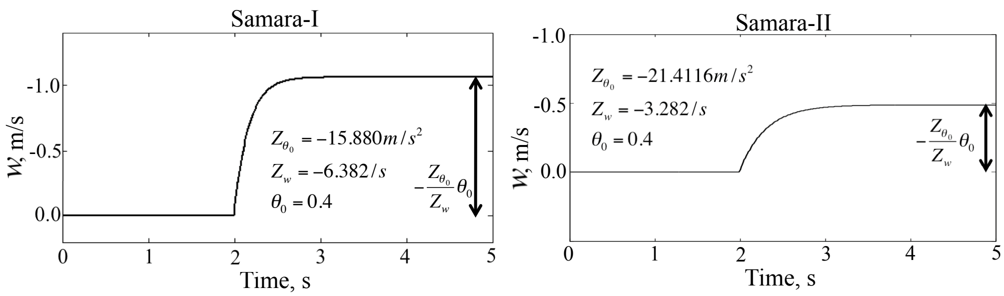

Figure 14. Mechanical samara heave response to a step input of collective pitch.

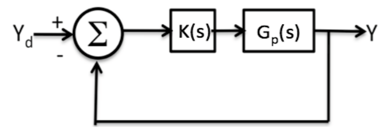

Figure 15. Prototypical Feedback Control Loop

A proportional plus derivative plus integral (PID) controller was chosen for feedback control of the Mechanical samara. A PID controller is given by the equation:

$$K(s) = K_p + K_d s + \frac{K_i}{s} \tag{38}$$

where K_p is the proportional gain and K_d is the derivative gain, and K_i is the integral gain. A PID controller feeds the error plus the derivative of the error forward to the plant. The proportional gain provides the necessary stiffness to allow the vehicle to approach the reference height. The P gain improves steady state error but causes overshoot in the transient response, whereas the derivative gain improves transient response. The integral term is proportional to both the magnitude and duration of the error in position, with the effect of eliminating the steady-state error. Using the ground control station setup described in Figure 8 for closed loop feedback control, several gain combinations were tested in order to find the PID gains which provided the best transient response to a change in reference height. The gains in Table 6 provide the best transient response. Figure 16 depicts a representative data set of a flight test with the implementation of the PID controller using the gains in Table 6, demonstrating that the actual height closely matches the reference height.

Table 6. PID Gains for feedback control.

Gain	samara-I	samara-II
K_p	0.211	0.344
K_d	0.889	0.133
K_i	0.028	0.020

The dashed line in Figure 16 is the altitude specified by the ground station, and the solid line is the vehicles vertical flight path. The characteristic over-damping in climb, and under-damping in descent, of samara-II is the result of gravitys effect on the vehicle. The settling time Ts of samara-I for a climbing maneuver is 1.03 s with no overshoot. A descending maneuver settles to 90% of the final value within 1.45 s with an overshoot of 22%. The smaller samara-II reached 90% of its final value in 1.7 s with an overshoot of 60% for a descent maneuver. The settling time for a climbing maneuver is 0.7 s with a 4% overshoot. It can be seen that the forces induced on the body from a change in collective pitch are substantial compared to the inertia of the vehicle, and increases in heave velocity are quickly damped after excitation.

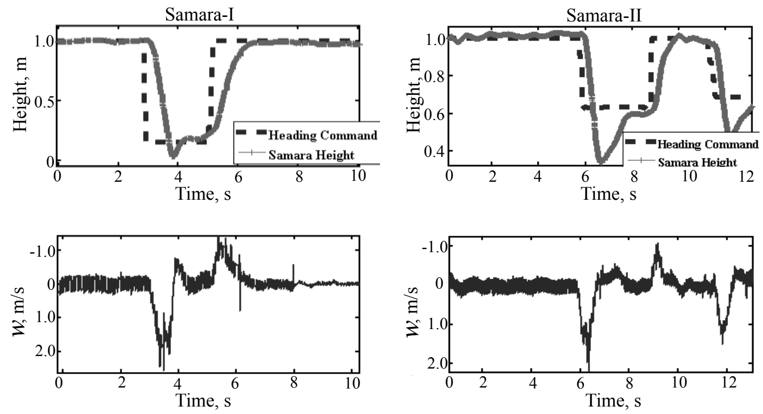

Figure 16. Implementation of PID control

VIII. Conclusion

This work presented the identification of a linear model describing the heave dynamics of two mechanical samara vehicles for use in future control and state estimation. A visual positioning system was used to collect flight data while the vehicles were piloted in an indoor laboratory. Eigenvalues of the heave dynamic model were estimated by two system identification packages. The identified parameters were used in simulating the vehicles response to heave and collective input perturbations as well as in the development of a PID controller. Closed-loop implementation of the derived controller was demonstrated which utilized the visual tracking system for position and velocity feedback. The characteristically under-damped response to a descent maneuver was found which differs from the critically damped response to an ascent maneuver.

IX. Acknowledgments

Thanks to the Faculty and staff of the University of Maryland for so graciously providing the facilities for these experiments. Thanks to Joe Conroy for his expertise on system identification, and for providing the electronics and feedback control interface. Thanks to Steven Gerardi for his assistance in the experimentation phase of work.

References

[1]Conroy, J., Humbert, J., and Pines, D., "System Identification of a Rotary Wing Micro Air Vehicle," *Journal of AHS*, 2009.

[2]Tischler, M. and Remple, R., *Aircraft and Rotorcraft System Identification: Engineering Methods with Flight Test Examples.*, American Institute for Aeronautics and Astronautics, 2006.

[3]B. Mettler, M. T., "System identication of small-size unmanned helicopter dynamics," *AHS 55th Forum*, 1999.

[4]Ulrich, E. and Pines, D., "Planform Geometric Variation, and its Effect on the Autorotation Efficiency of Mechanical Samara," *AHS64th Annual Forum*, 2008.

[5]Graham, F., *Monocopters*, Perigee Press, East Liverpool Ohio, 1999.

[6]Jameson, S., Allen, N., and Youngren, H., "SAMARAI Nano Air Vehicle - A Revolution in Flight." *DARPA contract W31P4Q-06-C-0324*, 2007.

[7]Baruh, H., *Analytical Dynamics*, McGraw-Hill, 1999.

[8]Stengel, R., *Flight Dynamics*, Princeton University Press, 2004.

[9]LabView, *Labview controller*, National Instruments, ni.com, 2008.

[10]Themathworks, *System Identification Toolbox*, Themathworks.com, 2008.

[11]Tischler, M., *Comprehensive Identification of FRequency Responses software (CIFER)*, Army Aeroflightdynamics Directorate (AFDD), 2008.

[12]Nise, N., *Control Systems Engineering, 4th ed*, John Wiley Sons, Inc., 2004.